Robust Lane Extraction From MLS Point Clouds Towards HD Maps Especially in Curve Road

Chengming Ye, He Zhao, Lingfei Ma, *Graduate Student Member, IEEE*, Han Jiang, Hongfu Li, Ruisheng Wang, *Senior Member, IEEE*, Michael A. Chapman, José Marcato Junior, *Member, IEEE*, and Jonathan Li, *Senior Member, IEEE*

Abstract—This article presents a semi-automated method to extract the lane features along the curved roads from mobile laser scanning (MLS) point clouds. The proposed method consists of four steps. After data pre-processing, a road edge detection algorithm is performed to distinguish road curbs and extract road surfaces. Then, textual and directional road markings such as arrows, symbols, and words, to inform drivers in necessary cases, are detected by intensity thresholding and conditional Euclidean clustering algorithms. Furthermore, lane markings are extracted by local intensity analysis and distance thresholding methods according to road design standards, because they are more regular along the road. Finally, centerline points on lanes are estimated based on the coordinates of extracted lane markings. Our method shows strong feasibility and robustness when creating high-definition (HD) maps from MLS data, by increasing the number of blocks in the curve and the distance threshold control in curved lane centerline extraction. Quantitative evaluations show that the average recall, precision, and F1-score obtained from four datasets for road marking extraction are 93.87%, 93.76%, and 93.73%, respectively. The generated lane centerlines are evaluated by overlaying them on manually labeled reference buffers from 4 cm resolution orthoimagery. The comparative study indicates that the proposed methods can achieve higher accuracy and robustness than most state-of-the-art methods.

Index Terms—High-definition map, mobile laser scanning, point clouds, road marking, centerline, lane-level navigation.
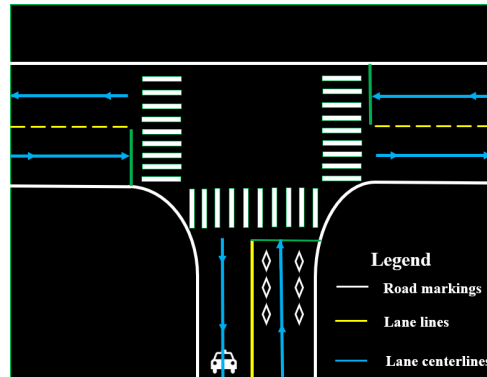
Fig. 1. The signage definitions of lane lines.

I. INTRODUCTION

PRECISE localization of autonomous vehicles (AVs) is crucial for public driving safety. Autonomous vehicles could conduct a series of catastrophic behaviors with inaccurate localization and route planning operations, such as driving on the opposite side of the road or illegally changing lanes [1], [2].

Autonomous driving systems sometimes identify sidewalks and maintenance lanes to be drivable or believe a destination is inside of a large obstacle [3]. To help such autonomous robots precisely perceive the world and achieve reliably environmental perception, multiple sensors are commonly employed in autonomous driving, including cameras, RAdio Detection and Ranging (RADAR), and Light Detection and Ranging (LiDAR) [4]–[6].

However, onboard sensors are not always reliable for the applications of precise trajectory design and detailed road information registration [7]. In general, autonomous vehicles need to recognize which lanes can be safely driven on, when turns to a curve, and when makes lane-changing decisions. It puts forward a very high demand for the road information extraction, especially in the more complex curve. In this article, we propose a new strategy using local and global intensity thresholds to extract lane lines (definitions showing at Fig. 1) with the control of distance threshold, and more blocks are generated in the curve to improve the precision of curved lane line extraction.

Different from conventional two-dimensional (2D) maps, High-definition (HD) maps are created using mobile laser scanning (MLS) data with the absolute localization accuracy

in the range of 10-20 cm [8]. MLS systems collect millions of 3D point clouds in complicated urban environments at a normal driving speed, which could represent detailed three-dimensional (3D) road network topologies [9]. Such highly precise HD maps can provide AVs with a longer sensing range and greater capacity to maneuver smoothly than onboard sensory devices [10]. It is well-known that the detection range of sensors is limited due to the presence of corners, ramps, and obstacles such as moving vehicles, pedestrians, and cyclists. If AVs can obtain auxiliary aids from a preloaded HD map, it can not only extend their sensing ranges beyond the reach of onboard sensors and know whether there are obstacles or sharp curves in the front of them, but also allows the decision-making subsystem to respond quite quickly [11].

By combining real-time sensory detection with prior knowledge, a preloaded map with rich metadata can transform the challenging sensor-based environmental perception task into a simplistic map-based localization mission. However, HD map-aided localization services still face several dilemmas. MLS system has great advantages in obtaining 3D HD maps with high precision and clarity. But point cloud processing is not an easy task, due to its massive data volume, unavoidable noises, high complexity, and occlusions [12]. For example, the size of an MLS dataset rendering 1 km length of an urban road acquired by RIEGL VMX-2HA or Trimble MX-9 systems is over 5 GB [9]. In addition, the inconsistent distribution of point density makes MLS data difficult to process. More challenge comes from performing prior knowledge (e.g., traffic restrictions) in road marking extraction and lane centerline generation [13]. Such dilemmas make efficient and robust lane feature recognition tasks from MLS point clouds challenge [14].

Currently, there is no commercial software with solid built-in functions that can handle large-volume of MLS point clouds. To solve such problems, this article attempts to develop a semi-automated approach for extracting valuable road features (e.g., road markings) and creating HD maps by employing MLS point clouds. More specifically, the significant contributions of this article are as follows: (1) an improved road curb detection algorithm for road surface extraction using MLS point cloud is proposed; (2) a novel semi-automated algorithm for road marking extraction by semantically and topologically analyzing road characteristics is developed; and (3) a novel algorithm is finally proposed for lane centerline generation, which supports sub-lane level navigation for autonomous vehicles. In summary, this article denotes a remarkable contribution to the research on lane feature recognition for HD map generation, which further conduces to the development of autonomous driving and vehicle-to-everything (V2X) technologies.

II. RELATED WORK

Currently, various methods have been developed for lane feature recognition and extraction in urban environments that are crucial to HD maps generation. This part provides an in-depth review and investigation from the perspectives of MLS point clouds. More detailed literature reviews were fully addressed in our recently published review article [9].

Generally, the commonly employed lane feature recognition algorithms using MLS point clouds are classified into two steps: road surface extraction (Section A) and road marking extraction (Section B).

A. Road Surface Extraction

The first step of extracting road features and creating 3D HD maps is road edge detection and road surface extraction. According to several studies, the road surface extraction methods can be classified into three groups: scan-line based, trajectory-based, and voxel-based.

Scan lines are usually produced based on the GNSS timestamp or scanning angle field when point clouds are organized by a given time interval. A scan line-based method was proposed in [15] to detect road surfaces by creating a moving window operator, which preliminary results achieved relatively high accuracy. By taking height differences between road surfaces and trajectories into consideration, a method was presented in [16] to extract road surfaces using a least-squares line-fitting algorithm. Although partitioning entire point clouds into multiple scan lines leads to computational complexity and algorithm applicability, detailed information contained within scan lines is still not sufficient for road curb detection in complex urban environments [17].

Additionally, trajectory data collected by MLS systems were generally used by dividing MLS point clouds into equally sized data blocks at certain time-wise or distance-wise intervals. In [18] and [19], the whole MLS point clouds were transversely partitioned into a series of point cloud profiles based on trajectory data, each profile was then sliced to produce pseudo scan lines with a specified width. Subsequently, road boundaries in each road data block were extracted based on the slope and height jumps between two neighboring points. Although road partition based algorithms could provide promising solutions for road surface extraction. The accuracy is heavily affected by the quality of trajectory data due to different laser scanning patterns. Road seeds were determined in [20] by detecting road curbs and separating the road surface from its surrounding environment. Meanwhile, the principal component analysis (PCA) was employed in [21] to detect road surfaces from the local neighborhood of the seed points. Furthermore, snake (a cubic spline-based algorithm) was used in [22] to fit road cross sections.

Other methods for road surface extraction mainly involve 3D geometric features filtering, surface growing, and voxel-based algorithms. An algorithm was presented in [23] for road surface segmentation from terrestrial laser scanning (TLS) data. In their approach, a fuzzy clustering method was applied to cluster raw TLS points. Then, a RANdom Sample Consensus (RANSAC) algorithm was applied to fit the linear clustered data. According to the density gradients of contiguous voxels, an approach was presented in [24] for road curb detection and noise removal. The experimental results showed a considerably high accuracy. However, the computational cost of voxel-based methods is relatively larger than other methods, especially for processing highly dense MLS point clouds in urban road networks.

Although most of the studies presented promising results, limitations inevitably existed in these approaches. For instance, some of the mentioned algorithms distinguished road points from non-road objects but failed to generate smooth road edges. Moreover, one more common limitation is that these algorithms mainly focused on a specific road type or a particular study area. For example, the algorithm proposed in [25] performed well for straight roads, but relatively weak for curved roads. In addition, thresholds used in these studies are highly dependent on prior knowledge and expert experience, which limits the extensive application of these algorithms.

B. Road Marking Extraction

Road markings are important lane features in traffic management systems, as they provide clear guidance and warnings for road participants (e.g., drivers, cyclists, and pedestrians). Most importantly, they also play an important role in developing intelligent transportation systems (ITS) and navigating AVs. Road markings are painted on asphalt pavements with particularly retro-reflective materials [21]. Accordingly, the approximately high reflectance is recognized as a unique characteristic to distinguish and derive road markings from road surfaces using MLS point clouds [26]. In fact, the laser pulse intensity values increase with the decrease of scanning ranges and incident angles between laser scanners and scanning targets [27]. Therefore, many algorithms for road marking extraction have been proposed mainly based on traditional approaches and deep learning (DL).

On the one hand, road markings can be extracted based on the 2D images derived from 3D point clouds. Such image-related methods are conducted by converting 3D point clouds into 2D georeferenced images based on the inverse distance weighted (IDW) interpolation algorithm [19]. Therefore, off-the-shelf image processing algorithms can be applied [28].

A multi-level thresholding segmentation method was presented in [29] to identify road marking candidates. With a set of local thresholds, connected contours were extracted from georeferenced images with inconstant luminance. A radius-rotating method [43] was developed to find road intersections and sliced roads from these places, then a total least squares line fitting was later used to obtain road centerlines. Another method [45], containing three key algorithms, namely, skewness balancing, rotating neighborhood, and hierarchical fusion and optimization (SRH), has extracted road centerlines from generated image in an urban environment with correctness and completeness of 91.4% and 80.4%, respectively. Subsequently, the support vector machine (SVM) algorithm was applied to classify the extracted road markings based on their morphological characteristics. The methods proposed in [19] and [25] both adopted an inverse perspective mapping (IPM) algorithm to transform the viewing angle of the image from the original position to a top-view perspective. The Otsu thresholding [30] was then conducted to segment various road markings from backgrounds (i.e., road surfaces). The extraction accuracy of these dimension reduction methods could be over 90%. Nevertheless, road markings were projected to a horizontal plane, which unavoidably results in an accuracy loss, especially for areas with large terrain variation. To deal with this problem, a multiple scale tensor voting (MSTV) algorithm was proposed in [31] to eliminate both false positive and false negative errors by employing a median-based filtering method.

Several studies focused on directly process point clouds for road marking extraction. An algorithm for lane marking extraction was developed in [32] using MLS point clouds. Apart from the intensity filter, the standard deviation of elevation was analyzed, and the lane markings were finally classified through Hough transformation. Another method called MTH [44], which represented three main famous algorithms, namely, Mean shift, Tensor voting and Hough transform. The mean shift algorithm was used for clustering road center points. To enhance salient linear features, the tensor voting algorithm was applied. Finally, the Hough transform algorithm was used to extract road centerlines. Recently, deep learning methods has attracted much attention in remote sensing field [33], [34]. A two step-wise method was developed in [35] to directly detect and classify road markings from MLS point clouds into stop lines, zebra crossings, road boundaries, arrows, rectangles, and centerlines. First, the large-size road markings were derived by using the multi-thresholding segmentation approach and spatial density filter. Then, the PCA and deep multi-layer perceptrons (MLPs) were conducted for the small-size road marking extraction and classification. A deep learning architecture was proposed in [36] for road marking extraction and classification. First, a modified U-shape neural network was applied for road marking segmentation. Subsequently, a multiscale convolutional neural network (CNN) based on hierarchical classification method was designed to classify various types of road markings, followed by a generative adversarial network (GAN) for road marking completion. Such deep learning-based methods for road marking extraction and classification have achieved state-of-the-art solutions. However, the limited availability of labeled point clouds is still the bottleneck for the widespread applications [37].

Furthermore, the intensity of point clouds is the most critical characteristics that can be used for extracting road markings. Distance-dependent thresholding is another common solution for achieving high accuracy in road marking extraction. For structured environments such as highways and viaducts, a single intensity filter can produce acceptable results, as there are no other features with high reflectance painted on the pavement. However, for complicated urban scenes, more additional attributes should be employed to deliver accurate road marking extraction results [38], [39].

III. Data Profiling

The MLS datasets used in this study were acquired by a RIEGL VMX-450 system [40]. Fig. 2 shows the geographic location and trajectory of the survey area. Table I indicates the detailed scanning parameter settings of such MLS system. The MLS surveys were conducted in Xiamen Island, Fujian, China (longitude 118°04'04"E, latitude 24°26'46"N). The data collection vehicle travels through the roads of interest at the speeds of up to 60 km/hr, resulting in the MLS point densities

This article has been accepted for inclusion in a future issue of this journal. Content is final as presented, with the exception of pagination.

4

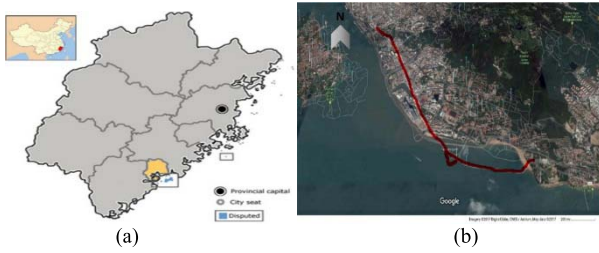IEEE TRANSACTIONS ON INTELLIGENT TRANSPORTATION SYSTEMS

Fig. 2. Study area in Xiamen Island, China. (a) Geographic location of Xiamen, China. (b) Trajectory of the study area.

TABLE I
SCANNING PARAMETERS OF THE RIEGL VMX-450 SYSTEM

Symbols	Descriptions	Values
S_S	Line scan speed	400 lines/sec
S_G	Vehicle speed	30-50 km/hr
L_D	Spacing between scan lines	9.71 cm
P_D	Spacing between points	5.98 cm
T_D	Target distance	30 m
L_I	Scan line incremental angles	0.1143°
PDen	Average point density	7,500 points/m2

Fig. 3. Workflow of the proposed method.

ranging from 7000-8000 points/m². The collected MLS point clouds were then processed and saved in multiple LAS files.

A total of four test datasets were used in this article. Dataset 1 is a simple urban road corridor that covers a small range of HuanDao Road with a length of near 30 m. The total number of points in Dataset 1 is 1,920,753 with a point density of 8000 points/m². Datasets 2, 3, and 4 are three segments of YanWu Bridge, covered by 6,758,030 points, 9,058,578 points, and 8,381,952 points, respectively. The lengths of these three segments are 176.5 m, 175.5 m, and 176.4 m, respectively. The average point density is 7500 points/m². Dataset 2 is a one-way two-lane road, while Datasets 3 and 4 are three-lane roads with lane reduction areas.

These four datasets contain a variety of road features, including different types of road markings, roadside trees, traffic signs, and buildings. Based on these four datasets, the performance of the proposed methods is tested and compared with other existing methods. Finally, orthoimage acquired from an unmanned aerial vehicle (UAV) was used to validate the experimental results of the proposed method.

IV. METHOD

In this section, we detail the proposed method for semi-automated extraction of lane centerlines. Such generated lane centerlines are further employed to facilitate the advancement of HD maps for autonomous vehicles.

A. Workflow of the Proposed Method

In order to deliver stable localization and navigation services for AVs in heavy traffic flow environments, the proposed method aims to extract essential lane features from MLS point clouds, including road edges, road surfaces, road markings, and lane centerlines. This method mainly contains four modules (see Fig. 3): data pre-processing, road edge and
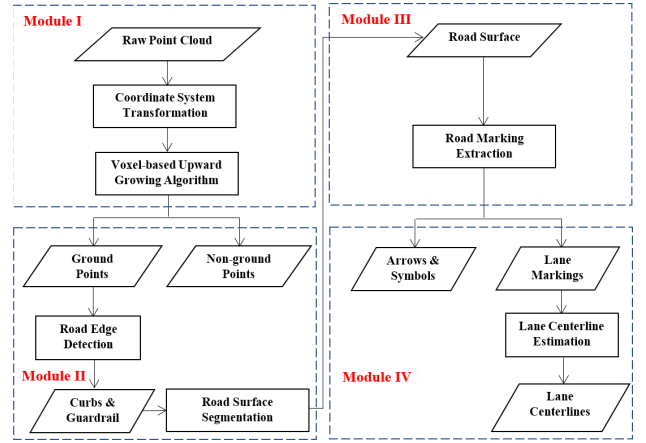
surface extraction, road marking extraction, and lane centerline estimation.

Specifically, Module I is designed for data pre-processing. A coordinate system transformation function is first implemented followed by a voxel-based upward growing algorithm [18] for non-ground points removal. Module II contains a road edge detection algorithm to extract road surfaces based on road design standards. Module III provides intensity analysis function based on outlier removal, and conditional Euclidean clustering algorithms to further extract both directional and textual road markings. Finally, Module IV contains a distance-to-road-edge algorithm for lane marking extraction, and lane centerlines are thus generated based on the coordinates of extracted lane marking points.

B. Module I: Data Preprocessing

Since the coordinate system of MLS system is arbitrary with a random user-defined origin point, a coordinate system transformation function is thus performed to fix the orientation of the vehicle frame so that the points can be more easily interpreted. The orientation of the vehicle frame is specified so that the x-axis towards the front of the vehicle, the y-axis points to the right of the vehicle, and the z-axis towards the top of the vehicle. Specifically, the coordinate system transformation is carried out by using:

$$X_{D_i} = D + (1+k)R(\varepsilon_x)R(\varepsilon_y)R(\varepsilon_z)X_{G_j} \quad (1)$$

$$\begin{cases} R(\varepsilon_x) = \begin{pmatrix} 1 & 0 & 0 \\ 0 & \cos\varepsilon_x & \sin\varepsilon_x \\ 0 & -\sin\varepsilon_x & \cos\varepsilon_x \end{pmatrix} \\ R(\varepsilon_y) = \begin{pmatrix} \cos\varepsilon_y & 0 & -\sin\varepsilon_y \\ 0 & 1 & 0 \\ \sin\varepsilon_y & 0 & \cos\varepsilon_y \end{pmatrix} \\ R(\varepsilon_z) = \begin{pmatrix} \cos\varepsilon_z & \sin\varepsilon_z & 0 \\ -\sin\varepsilon_z & \cos\varepsilon_z & 0 \\ 0 & 0 & 1 \end{pmatrix} \end{cases} \quad (2)$$

where X_{D_i} and X_{G_j} are the coordinates of MLS point clouds in the transformed coordinate system and original coordinate
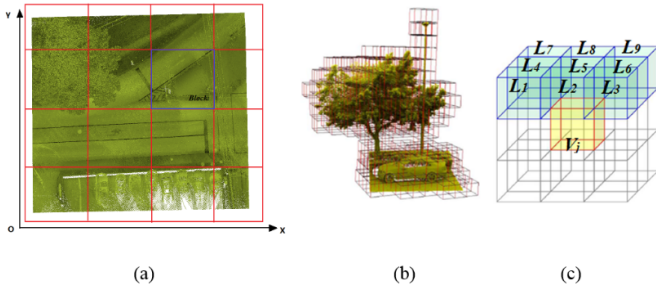
Fig. 4. The voxel-based upward-growing algorithm. (a) raw point cloud segmentation process, (b) Octree Spatial Index in local blocks, and (c) voxel-based upward growing pattern.

system, respectively. $D = (\Delta X, \Delta Y, \Delta Z)$ is the transformation matrix, and k is the scaling factor denoted as the ratio between the original and transformed coordinates. Where ε_x, ε_y, ε_z are the three rotation angles of the 3D coordinate system and $R(\varepsilon_x)$, $R(\varepsilon_y)$, $R(\varepsilon_z)$ are their corresponding rotation matrix. To fix the orientation of x-axis and y-axis, two consecutive trajectory points are selected as reference points to calculate the rotation angle.

Moreover, this article only focusses on extracting on-road information, the non-ground points have become relatively redundant. Accordingly, a voxel-based upward growing method [18] was employed to identify and separate non-ground points from ground points such as canopies, buildings and traffic signs for computational efficiency enhancement.

Fig. 4 illustrates the detailed procedure of the voxel-based upward growing approach. First, as shown in Fig. 4(a), the raw point clouds are horizontally segmented into blocks. The width of each block is afterward determined by the size of test datasets. Instead of globally processing the entire point clouds, this process can greatly reduce the influence of ground undulations. Then, the points in each data block are further divided into a series of voxels. The certain width of voxels is calculated by the average point density using octree spatial index (see Fig. 4(b)). Next, each voxel will grow upward toward its 9 adjacent voxels. As shown in Fig. 4(c), 9 neighbors of voxel V_j are voxels $L_1, L_2 \ldots L_9$. Subsequently, the upward growing algorithm will regard its 9 neighbors of voxel V_j as new starting points and continue to grow upward following the same pattern. This process will not terminate until all voxels have no adjacent voxels.

During the upward growing process, the voxels with the maximum local height values in each growing region are determined. Finally, the following criteria are used to judge whether a voxel belongs to ground voxel or non-ground voxel:

$$\begin{cases} Non-ground\ voxels, & if\ H_{global} > H_e\ or\ H_{local} > H_g \\ Ground\ voxels, & if\ H_{global} \leq H_e\ or\ H_{local} \leq H_g \end{cases} \quad (3)$$

where H_{global} denotes the global height value of a voxel, which is defined as the height difference between the certain voxel and the lowest voxel in the entire point cloud. H_{local} is the local height value of a voxel, which is determined as the height difference between the certain voxel and the

lowest voxel in a certain block. H_e represents a global ground undulation threshold, which is calculated by the maximum z value of the entire test dataset. H_g denoted by the maximum z value in a specific growing region indicates a local ground undulation threshold.

Accordingly, the voxels will be regarded as ground voxels, if either the global height value H_{global} is less or equal than the global ground undulation threshold H_e, or the local height value H_{local} is less or equal than the maximum z value H_g. As demonstrated in this article, such voxel-based upward growing procedure by embedding the dynamic sizes of point cloud blocks and upward growing voxels, can save more computational power than directly using elevation thresholding based methods [9]. Most importantly, the integrity of ground point clouds is completely retained without any information loss.

C. Module II: Road Edge Detection and Road Surface Extraction

Road curbs are constructed as road boundaries that separate sidewalks and green belts from road surfaces [41]. Therefore, an improved curb-based road surface extraction method is proposed, which consists of three key steps: road curb detection, road edge refinement, and road surface extraction.

1) Road Curb Detection: Instead of directly processing the entire dataset, processing 3D points in each local data block can considerably reduce the negative effects of road undulations. Thus, the segmented ground point clouds are first partitioned into data blocks based on a user-defined interval (L) perpendicular to the vehicle trajectory. The key idea is setting a proper segmentation interval in order that each block can have the least but sufficient points, which means one curb candidate points could be detected at least on both sides of the local block. Otherwise, the length of these blocks should be increased. In this article, the total number of blocks ranges from 30 to 500 depending on the size and characteristics of test datasets.

Consequently, ground points are divided into a series of local blocks after data segmentation. In each block, the proposed algorithms detect curb points based on two criteria: slope and height differences. According to the road design rules and visual inspection of the test datasets, pavements are typically higher than roadways in a neighborhood with a 7 - 15 cm elevation jump. Moreover, slopes at the pavement shoulders are larger than those of continuous points on roadways. Fig. 5 presents typical road curbs with intensity information from MLS point clouds. Therefore, based on both slope jumps and height differences, the following two criteria are defined and applied to determine whether a point p_i is a curb point:

$$\forall P_i : \begin{cases} curb\ candidate, & if\ (S_{slope} > S_T \\ & \&\ (G_{min} \leq G_i \leq G_{max})) \quad (4) \\ non-curb\ point, & otherwise \end{cases}$$

where S_{slope} is the slope of two consecutive points, S_T is a user-defined slope threshold, G_i denotes the elevation difference between a point and its adjacent point in a pseudo
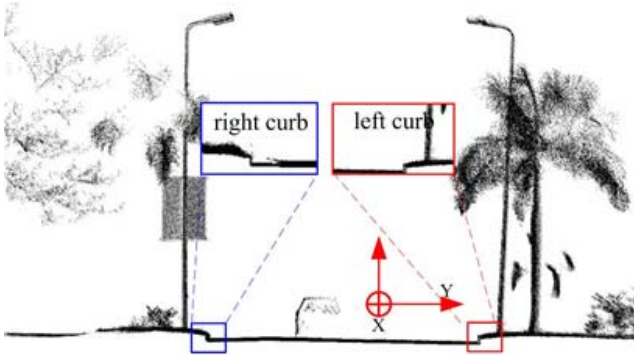
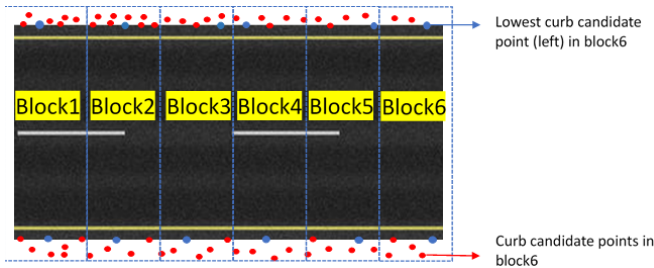Fig. 5.   Illustration of road curbs in MLS point clouds.

Fig. 6.   Illustration of the proposed curb extraction method.

scan line. G_{min} and G_{max} are the minimum and maximum elevation difference thresholds, respectively. S_{slope} is calculated by:

$$\begin{cases} S_{slope} = \arctan(\dfrac{Z_{i+1} - Z_i}{\sqrt{(X_{i+1} - X_i)^2 + (Y_{i+1} - Y_i)^2}}) \\ S_{slope} \in (\dfrac{-\pi}{2}, \dfrac{\pi}{2}) \end{cases} \quad (5)$$

where (X_i, Y_i, Z_i) and $(X_{i+1}, Y_{i+1}, Z_{i+1})$ are the coordinates of two consecutive points in a pseudo scan line. The revised algorithms calculate slope and elevation differences of any two consecutive points in each scan line. Once a point's slope and elevation difference match the given thresholds, this point is thus considered as a curb candidate. By using this strategy, several curb candidates are extracted within each data block. Subsequently, a quick sorting algorithm is performed to sort all curb candidates in data blocks based on their elevations. The lowest points on each side of the block are considered as the bottom points of road curbs. Fig. 6 illustrates the principle of the revised road curb extraction method. The red points are curb candidate points in local blocks and the blue points represent the lowest curb candidate points on each side of the block.

2) Road Edge Refinement: Different from most existing methods, in this article, the positions of lane marking points are determined by calculating their distances to the extracted road edges. Therefore, the accuracy of extracted curb points is of great significance. All extracted curb points are expected to be the bottom of curbs or guardrails. However, it is inevitable that some extracted points lead to slight deviations. Thus, a road edge refinement method by employing RANSAC is proposed to remove outliers.

The robustness of RANSAC makes it commonly applied. It keeps searching for better models until a user-defined iteration number is reached. In this article, since the number of the extracted curb points is usually nearly 300 with few outliers in our datasets, the upper bound of iterations is set to be 1,000.

It is noteworthy that if the number of curb points is not enough after refinement, a point interpolation method is implemented to interpolate points between consecutive curb points. The midpoints of any two consecutive curb candidates are regarded as new curb candidates until a pair of curb points are found within each local data block. Accordingly, a B-spline curve fitting algorithm is conducted to fit the extracted road edge in the XY -plane.

3) Road Surface Extraction: Finally, two curb points are extracted on both sides in each block. Based on the positions of these curb points, linear functions that pass any two consecutive curb points can be calculated. Therefore, any two consecutive curb points could generate a local edge line. Consequently, in each block, the points located in the inner side of the corresponding edge line are determined as road surface and accordingly extracted.

D. Module III: Road Surface Information Extraction

Different road markings have various characteristics, such as widths, lengths, shapes, colors, and positions. In this article, two algorithms are developed with each focusing on different types of road markings. On one hand, a clustering algorithm based on morphological analysis is developed to extract directional and textual road markings including arrows, symbols, and words. On the other hand, a distance-to-road-edge thresholding approach using road construction standards is proposed to extract lane markings, such as solid and broken lines.

1) Directional and Textual Road Marking Extraction: With extracted road surface points, a directional and textual road marking recognition framework is proposed. It consists of three processes: intensity analysis, statistical analysis-based outlier removal, and conditional Euclidean clustering.

Due to the near-infrared wavelength of laser pulses, road markings have higher reflectance than unpainted road surfaces. Therefore, a global intensity filter is first applied, which detects road markings depending on intensity information. The observation is defined as:

$$\forall p_i : \begin{cases} Road\ marking\ candidates, & if\ (I_{min} \le I_i \le I_{max}) \\ non-marking\ points, & otherwise \end{cases}$$

$$(6)$$

where I_i is the intensity values of MLS points. I_{min} and I_{max} are the minimum and maximum intensity thresholds, respectively. If a point's intensity value is within the predefined range, this point is then determined as a road marking candidate. However, the point intensity largely depends on the scanning range and incidence angle of laser beams, which contributes to a phenomenon that point intensity gradually fades from the vehicle trajectory to its both sides [31]. Thus, local optimal thresholds are required to be adaptively estimated.

Specifically, I_{min} is usually set as small values to avoid the error of omission.

However, noise inevitably exists in MLS point clouds after using the global-scale intensity road marking extraction method. Such noisy points complicate the estimation of local point cloud characteristics, leading to erroneous values, which in turn could cause point cloud registration failures. In this article, most of the noise are isolated points and point mutations in local neighborhoods. Thus, a statistical outlier removal (SOR) algorithm is applied. More specifically, the SOR algorithm firstly attempts to find the K neighboring points from certain points of interest, where K is a user-defined threshold based on the average point density. If there are no enough neighbors within a stated radius, the point is considered as an outlier and removed from the point cloud. Furthermore, if the K-nearest points of a certain point are founded in a specified area, the mean distance from this point to its neighbors is calculated. The SOR algorithm assumes that the distribution of the mean distance of all points should follow Gaussian distribution, and the points outside an interval defined by the clustering method [16] is performed. Based on the mean and standard deviation of global distances are considered as outliers and eliminated from the dataset. As consequence, filtering out noisy points can enhance computational efficiency prior knowledge (e.g., heights, sizes, and widths) of road markings, and relatively large clusters (e.g., arrows and words) are distinguished by removing small clusters (e.g., straight lines and noise). A width threshold denoting the difference between the maximum and minimum y values of point clouds is applied to eliminate irrelevant clusters and improve road marking extraction accuracy.

Although outliers are filtered out, points belonging to the same object are still isolated and unorganized, and there are no topological relationships among points. Therefore, to distinguish specific objects (e.g. arrows) and organize discrete points into semantic clusters, a revised conditional Euclidean clustering (CEC) method [16] is performed based on the prior knowledge (e.g., heights, sizes, and widths) of road.

2) Lane Marking Extraction: Next, a distance-to-road-edge method is proposed for lane marking extraction. By taking refined road edges as benchmarks, the positions of lane marking points are determined by calculating the distances from each point to road edges. The thresholds used in this algorithm are defined by road design standards, which regulates the widths of road markings, lanes, marginal strips, and road shoulders.

The distance-to-road-edge algorithm initially considers the refined curb points as (see red points in Fig. 7) control points and then segments data into a considerable number of blocks. Every two consecutive curb points will generate one block, and a linear function is calculated based on the coordinates of two consecutive curb points.

This segmentation process enables the proposed algorithm to process a minimal set of data in local blocks, thus reducing the influence of errors on global scale. After segmentation, a searching window first moves from the two curb points in each local block, and then searches for points whose distances to the generated edges are within a predefined range. Meanwhile, a point intensity thresholding is applied to detect
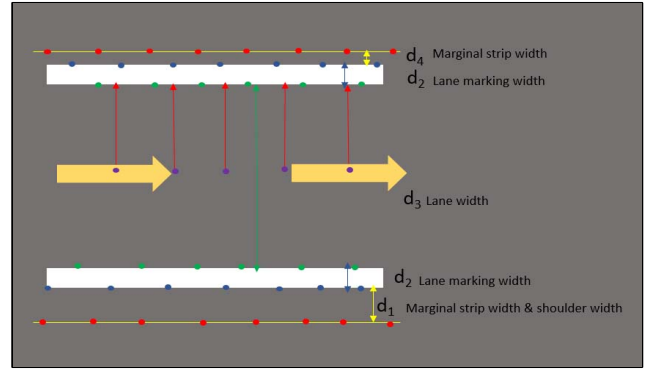

Fig. 7. Distance thresholding.

points with high retro-reflectance values in certain strips. The criteria for detecting lane markings are described as follows:

$$\forall p_i : \begin{cases} Lane\ point, & if\ (I_{min} \leq I_i \leq I_{max}) \\ & \&\ (d_{min} \leq d_i \leq d_{max}) \\ Non-lane\ points, & otherwise \end{cases} \quad (7)$$

where I_i is the intensity value of a point. I_{min} and I_{max} are the minimum and maximum intensity thresholds, respectively. d_i is the distance from a point to the generated road edge in the local block. d_{min} and d_{max} are the minimum and maximum distance thresholds, which are preset according to road design standards.

Moreover, according to the Code for Layout of Urban Road Traffic Signs and Markings of China (GB 51038 C 2015), lane widths are at least 3.5 m for urban roads with a speed limit of 60 km/hr. Additionally, marginal strip widths range from 0.5 m to 0.75 m for urban roads, and shoulder widths range from 1.5 m to 2.5 m for the test roads. Furthermore, the width of lane markings in the study area is 0.15 m. Thus, d_{min} and d_{max} are usually set at 0.5 m and 0.9 m, respectively.

Consequently, points with certain intensity values and within specific regions are extracted as lane markings. The nearest and farthest points on lane markings are considered as the outer edge and inner edge of the lane marking and separately extracted. Finally, as shown in Fig. 7, lane centerline points are estimated by finding points with a certain distance $(d_1 + d_2 + d_3/2)$ to the right road edge. The equation of the distance from a point to a line is described as follows:

$$d = \frac{|ax_0 + bx_0 + c|}{\sqrt{a^2 + b^2}} \quad (8)$$

where d is the distance from a point to a line, (x_0, y_0) represents the 2D coordinate of a point, and a, b, and c are the coefficients of a linear function, which is estimated by two consecutive curb points in local data blocks.

This method can produce promising results, especially for straight roads. It should be noted that when deals with curves, partitioning data into more strips is a useful approach to improve extraction accuracy. The smaller the length of each block, the more similar the shape of the rectangle and its corresponding arc. Fig. 8 shows the proposed method applied to curve roads. Fig. 8 (a) shows a curved road section segmented
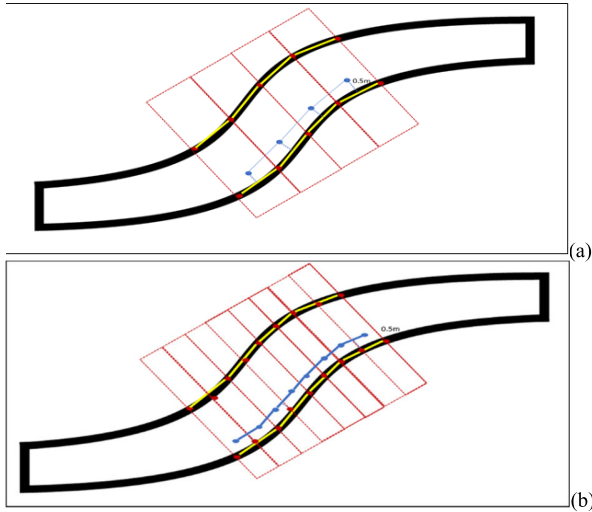
This article has been accepted for inclusion in a future issue of this journal. Content is final as presented, with the exception of pagination.

8   IEEE TRANSACTIONS ON INTELLIGENT TRANSPORTATION SYSTEMS

Fig. 8. Lane marking extraction using different blocks in curves. (a) 4 blocks, (b) 8 blocks.

Fig. 9. Centerline estimation.

into 4 blocks (red rectangles), while Fig. 8(b) shows an 8-block segmentation result of the same curve. Red points are the extracted curb points, yellow lines are the local road edge lines connected by consecutive curb points, and blue points denote the detected lane marking points. Therefore, the smoothed lane marking extraction results could be obtained by partitioning data into more slices of blocks.

E. Module IV: Lane Centerline Estimation

To calculate the coordinates of lane centerline points, the same segmentation procedure as mentioned before is hereby implemented. The extracted lane markings are segmented into hundreds of blocks, where the center points of lane markings on both sides in each data block are extracted. The coordinates of the center points in each block are calculated by:

$$C\left(X_C, Y_C, Z_C\right)=\left(\frac{X_{max}+X_{min}}{2}, \frac{Y_{max}+Y_{min}}{2}, \frac{Z_{max}+Z_{min}}{2}\right) \quad (9)$$

where X_{max}, X_{min}, Y_{max}, Y_{min}, Z_{max}, and Z_{min} are the maximum and minimum values of x, y, and z for each cluster in the local block, respectively.

Two center points are extracted in each local block with one on each lane marking cluster. Similarly, the coordinates of lane centerline points are estimated by calculating the coordinate mean of two extracted center points in each local block. Generally, a point cloud is segmented into hundreds of blocks, thus producing the same number of lane centerline points. However, for broken lines and faded lane markings, a center point interpolation method is applied to interpolate center points in empty areas until enough lane centerline points are generated. Fig. 9 manifests the principle of the proposed lane centerline estimation method.
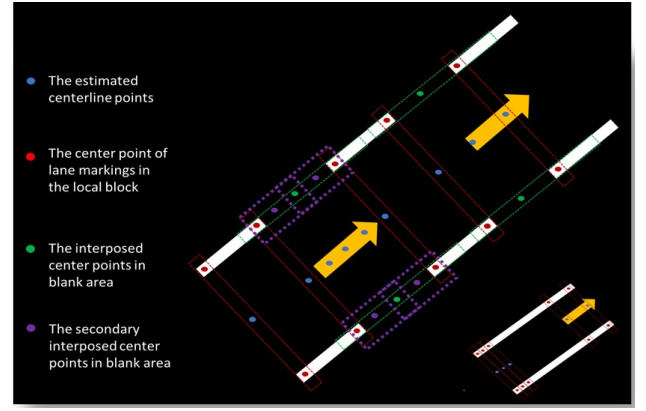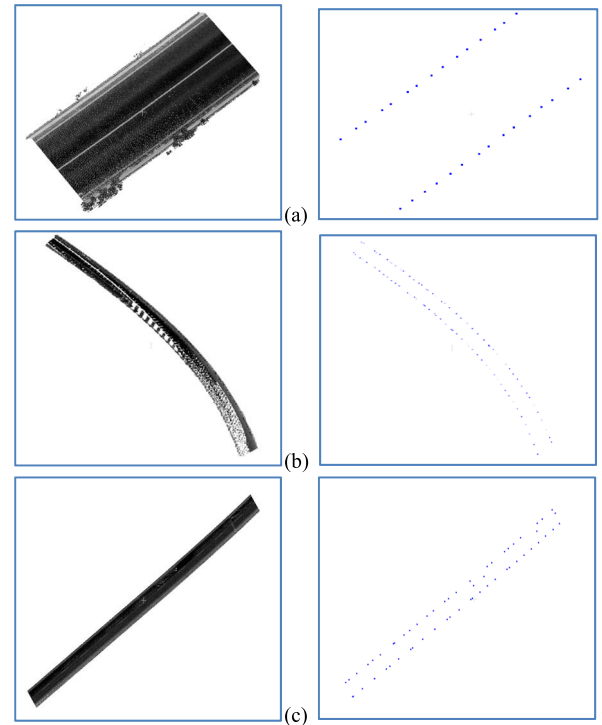

Fig. 10. Road curb detection results in this paper, three datasets (left) and refined curb points (right). (a) Dataset 1; (b) Dataset 2; (c) Dataset 3.

V. Results and Discussion

A. Road Curb Detection and Road Surface Extraction

In this article, road surfaces were extracted by detecting curb points as road boundaries. Three critical parameters were predefined according to prior knowledge about road design standards, namely, minimum height difference $G_{min} = 7$ cm, maximum height difference $G_{max} = 30$ cm, and slope $S_{slope} = 70°$. Fig. 10 presents the non-ground point removal and road edge refinement results of Datasets 1, 2, and 3.

Based on the coordinates of extracted road curb points, points located between the left and right road edges are considered as road surfaces and therefore extracted. It is noted that a road edge is defined as the straight line or curve that passes the two nearest curb points. As mentioned before, partitioning data into more pieces of block can improve
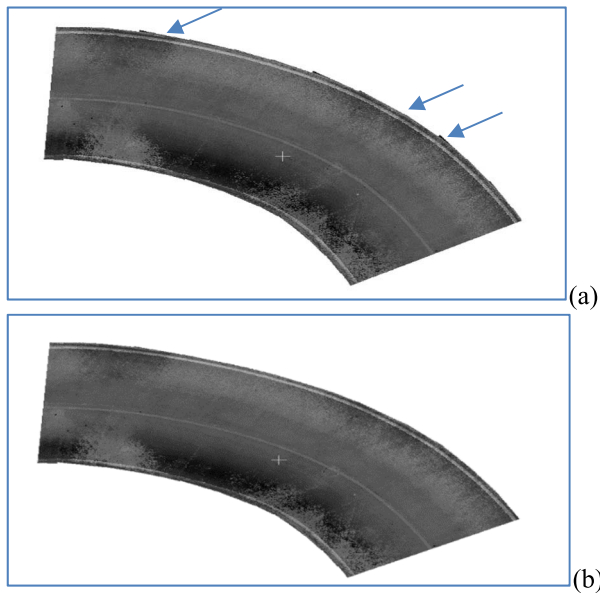
Fig. 11. Curved road surface segmentation results obtained using (a) 50 blocks and (b) 300 blocks.

the performance of the proposed algorithm. This strategy is particularly beneficial to curved roads, as the proposed algorithm extracts road surfaces in each local block with a pair of local road edges as references. If the area of each block is not small enough, the estimated road edge could not fit the real road edge. As shown in Fig. 11, more smooth road edges can be obtained based on the 300-block segmentation, see Fig. 11(b), compared to the 50-block segmentation, see Fig. 11(a). It indicates that the more blocks are used, the more accurate road edges could be extracted.

B. Road Marking Extraction

As shown in Fig. 12, the proposed road marking extraction algorithm was tested on the four datasets, which contained different types of road markings including arrows, symbols, words, lanes, and hatch markings. To achieve the best performance, local optimal thresholds were estimated based on the characteristics of different datasets. The distance thresholds were determined by road design standards. According to the Code for Layout of Urban Road Traffic Signs and Markings of China (GB 51038-2015), d_{min} was set to 0.5 m, and d_{max} was set to 0.9 m for roads without shoulders. For roads decorated with shoulders, $d_{min} = 1.5$ m, $d_{max} = 2.75$ m for the right side, and $d_{min} = 0.5$ m, $d_{max} = 0.9$ m for the left side, respectively. Apart from distance-based thresholding, intensity information is also utilized to detect lane marking points. Generally, the minimum intensity threshold I_{min} was set as 23,000, and the maximum intensity threshold I_{max} was set to be 40,000 based on visual interpretation of test datasets.

As shown in Figs. 12 and 13, most lane markings were successfully extracted from road surfaces. However, some extracted road markings in Fig. 12 were incomplete (see highlighted in the red rectangles A and B). The missing parts were primarily caused by the occlusions of large obstacles, as laser
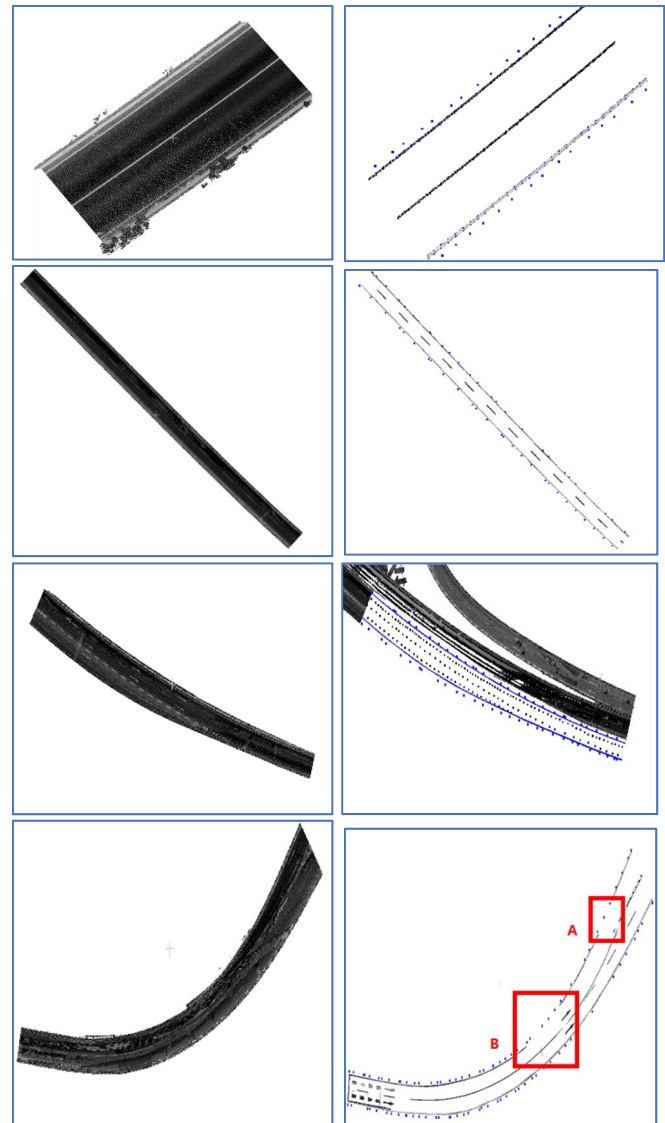

Fig. 12. Extracted lane markings and key points: four datasets (left) and extracted lane markings (right).

pulses cannot reach the shadows of the obstacles. Another reason is that some road markings have been painted on the road surfaces for decades without routine maintenance. Thus, road marking decay has been caused by heavy-duty trucks and salt dissolution in snow season. In summary, the proposed lane marking extraction method delivered promising results.

C. Lane Centerline Estimation

The coordinates of lane centerline points were estimated depending on the coordinates of the extracted lane marking points on both left and right sides. In this article, Wz was set to 2.0 m for Dataset 1, Dataset 2, Dataset 3, and 0.5 m for Dataset 4 based on experiments assessments. Wz is a predefined width threshold that denotes the width of each block. After extracting desired road information, the generated LAS file was converted to Shapefile format and further processed in ESRI ArcGIS software. Finally, discrete lane centerline points were linked using an XY-Line tool in ArcGIS to create smooth lines (see Fig. 14). In addition, the map can be converted to other
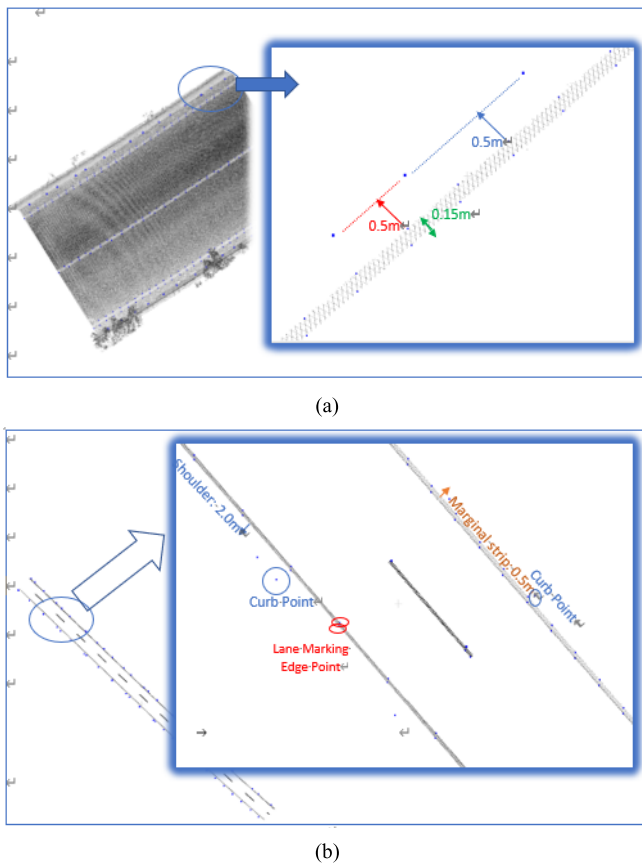
(a)

(b)

Fig. 13.   Detailed sections of the extracted lane markings and key points. (a) Test dataset 1. (b) Test dataset 3.

types of user-defined formats. Thus, the HD map prototype was developed for the localization and navigation missions of autonomous vehicles, as shown in Fig. 15.

D. Accuracy Assessment

Furthermore, an accuracy assessment was implemented to evaluate the performance of the proposed methods. Three criteria including *Recall*, *Precision*, and *F1-score* were used to conduct the accuracy assessment. The expressions are defined as follows:

$$Recall = T_p / (F_N + T_P) \tag{10}$$

$$Precision = T_P / (F_P + T_P) \tag{11}$$

$$F_{1-score} = \frac{2 \times Precision \times Recall}{(Precision + Recall)} \tag{12}$$

where T_P represents true positive, F_P denotes false positive, and F_N indicates false negative classification outputs. In this article, the recall addresses the completeness of the extracted road markings, while the precision shows the valid percentage of these extracted road markings. Moreover, $F1$-score describes an overall score by taking both precision and recall into consideration. More specifically, T_P denotes the number of correctly classified road marking points, F_P represents the quantity of noisy points that are misclassified to lane marking points, and F_N indicates the quantity of lane marking points that are misclassified to outliers.

(a)

(b)
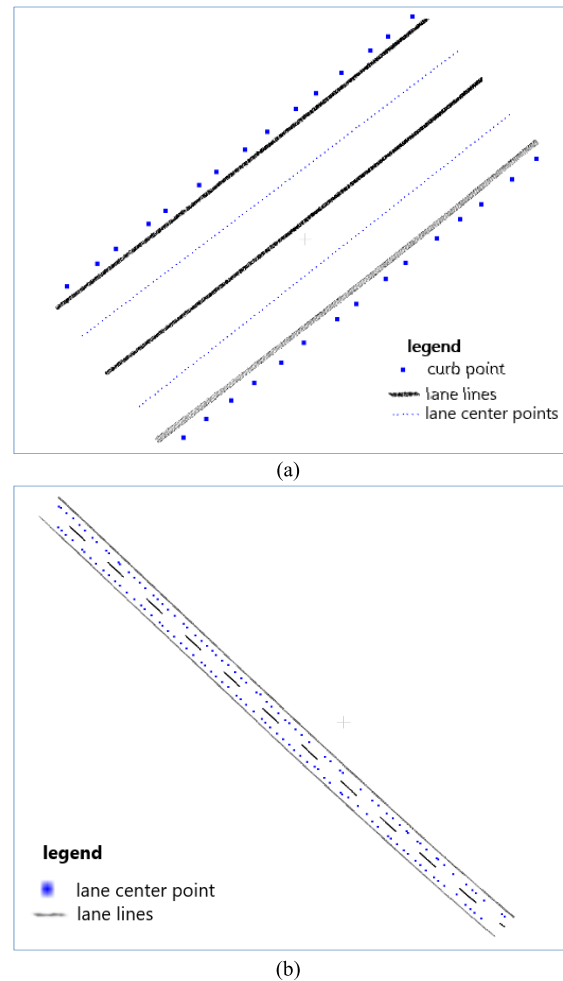
Fig. 14.   The estimated lane centerlines in this article. (a) Test dataset 1. (b) Test dataset 2.
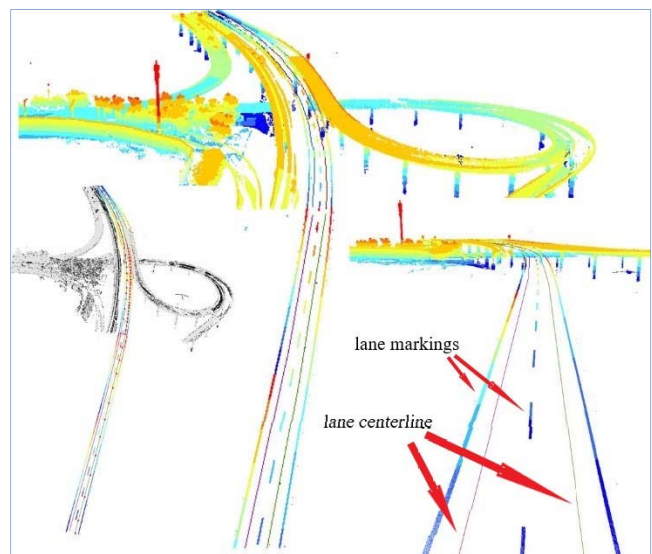

Fig. 15.   A 3D HD map prototype created in this article.

A set of reference pixels for each dataset was manually labeled using UAV orthoimagery in ArcGIS v10.3. Additionally, the MLS point clouds were aligned to the same coordinate system (UTM) with an UAV orthoimagery. Then, the extracted road markings were overlapped with UAV images in ArcGIS.
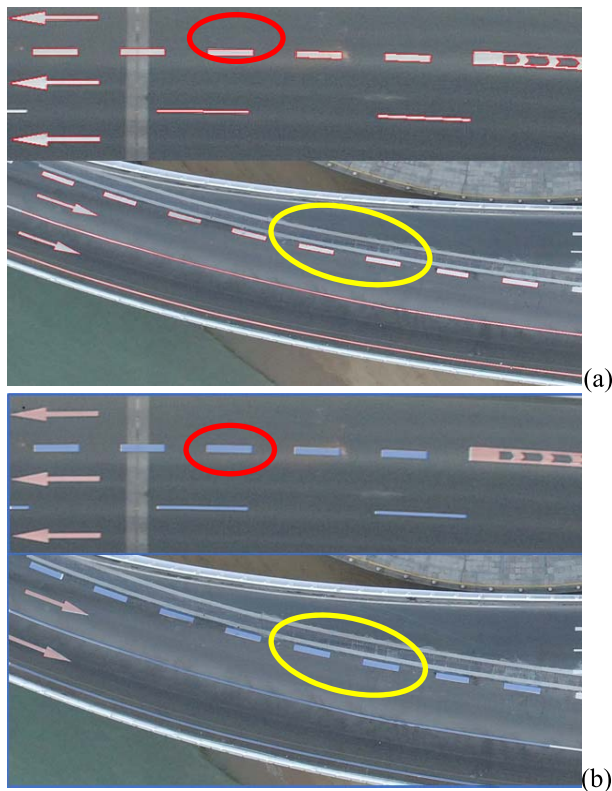
Fig. 16. Validation of the extracted road marking overlapped with orthoimage. (a) Manual interpreted road marking polygons, (b) orthoimage overlapped by extracted road markings.

TABLE II

QUANTITATIVE ASSESSMENT OF ROAD MARKING EXTRACTION

Dataset	Precision (%)	Recall (%)	F_1-score
1	97.78	96.57	0.9717
2	95.65	95.54	0.9559
3	96.83	89.72	0.9314
4	85.21	93.22	0.8904
Average	93.87	93.76	0.9373

After pixel analysis, *Precision*, *Recall*, and *F1-score* were calculated to express the accuracy of experimental results. Fig. 16(a) presents the manual interpreted road marking polygons, and Fig. 16(b) shows the validation results of the proposed road marking extraction algorithm with the assistance of 4 cm resolution UAV orthoimagery.

As shown in Table II, the proposed road marking extraction method can achieve 93.87% in precision, 93.76% in recall, and 93.73% in F1-score. Both precision and recall of Dataset 1 are very high, as Dataset 1 is a short and straight road without barriers or obstacles. Similarly, Dataset 2 is a straight road corridor of YanWu Bridge and yet much longer than Dataset 1. The recall of Dataset 3 is relatively low, as lane reduction areas exist. The number of lanes is reduced from three lanes to two lanes in the same direction. As the effective width of roads is decreased, it is challenging to estimate local optimal thresholds for lane reduction areas. Moreover, the recall for Dataset 3 is low due to misclassification, which some road surface points are misclassified into road marking points. In Dataset 4, two moving vehicles block parts of road

Fig. 17. Lane centerline validation results using user-defined buffer zones.

markings on the left side of the road, thus resulting in low precision. Moreover, the occlusions of shadows and obstacles are common shortcomings of MLS systems, as laser pulses cannot penetrate most objects.

Furthermore, the estimated lane centerlines were overlapped with an UAV orthoimagery. Buffer zones with the width of 10 - 30 cm were manually drawn in base maps as references, and the experimental results were thus evaluated by determining whether the estimated lane centerlines located in the buffer zones. Otherwise, the offsets should be calculated. All estimated lane centerlines were evaluated through manual inspection. The experimental results demonstrate that the estimated lane centerlines of Datasets 1, 2, and 3 can correctly match the real centerlines, located in 10-cm-wide buffer zones. The simulated lane centerline of Dataset 4 had a small deviation due to some misclassification and incomplete extraction of road markings. The maximal localization error is approximately 15 cm. Thus, a 30-cm-wide buffer zone was defined to cover all lane centerlines of Dataset 4. It is well-known that the width of vehicles is normally less than 2 m, and the width of a single traffic lane in China is at least 3.5 m. Thus, a 0.4 m lateral clearance enables to ensure driving safety. According to the Enhanced Digital Mapping Project Final Report released by the Department of Transportation of the USA, the localization accuracy specification of lane centerline estimation is 0.3 m. Therefore, all generated lane centerlines in this article meet national and industrial standards. Fig. 17 presents the lane centerline validation results of Dataset 3.

E. Comparative Study

To evaluate the performance of the proposed methods, a comparative study was conducted. We compared the proposed road edge detection method with the one presented in [31]. Remarkably, the method presented in [31] and the proposed method in this article achieved similar precision, recall, and F1-score values for Dataset 1. But for Dataset 4, the proposed method is more superior to the one presented in [31]. The comparison results demonstrate that the method presented in [31] is not capable of handling urban road scenes with horizontal curves and obstacles. Table III presents the quantitative evaluation results of these two methods.

TABLE III
ACCURACY ASSESSMENT RESULTS USING DIFFERENT
ROAD EDGE DETECTION METHODS

Method	Dataset	Recall (%)	Precision (%)	F1-score (%)
Guan et al. [31]	1	95.20	96.54	95.86
	4	83.43	85.21	84.31
Our method	1	95.61	96.32	95.96
	4	92.91	95.06	93.97

TABLE IV
ACCURACY ASSESSMENT USING DIFFERENT ROAD MARKING

Method	Dataset	Recall (%)	Precision (%)	F1-score (%)
Chen et al. [42]	1	91.03	75.67	82.64
	4	92.37	71.43	80.56
Yu et al. [18]	1	92.05	93.24	92.64
	4	91.13	93.02	92.06
Cheng et al. [25]	1	96.11	89.07	92.46
	4	98.06	91.12	94.46
Our method	1	92.56	95.35	93.93
	4	90.53	95.71	93.04

The proposed road marking extraction method was compared with some existing methods, including those methods presented in [18], [25], [42]. In [25], MLS point clouds were firstly converted to 2D georeferenced intensity images. Then, they extracted road markings from such 2D images with the assistance of software including ENVI and ArcGIS. However, in [18] and [42], the proposed methods directly extracted road markings from MLS point clouds.

Table IV indicates the quantitative evaluation results. It is perceived that the proposed method achieves the highest precision among the four methods. However, our approach is inferior to the method presented in [25] method in terms of recall. Consequently, the outlier removal algorithm and clustering algorithm certainly require further refinement. Moreover, the proposed method outperforms both methods presented in [18] and [42] in both precision and recall. The method presented in [42] only focuses on line-shaped markings. Additionally, the methods proposed in [18], [25] rarely have inconstant intensity and blurring data problems, thus achieving relatively high precision.

VI. CONCLUSION

In this article we have presented a semi-automated method to extract lane centerlines from MLS point clouds. The proposed method first removes non-ground points using a voxel-based upward growing algorithm. Then, a road edge detection algorithm is performed to detect road curbs for road surface segmentation. Next, road markings including arrows, symbols, and words, are preliminarily detected using a global intensity filter. Semantic clusters of these textual and directional road markings are afterward extracted by statistical analysis outlier removal algorithm and conditional Euclidean clustering algorithm. Moreover, lane markings are derived by local intensity analysis and distance-to-road-edge thresholding methods based on road design standards. Finally, centerline

points located between two adjacent lanes are estimated based on the coordinates of extracted lane markings. Accordingly, HD maps with precise road boundaries, road markings, and lane centerlines are created.

Four datasets were tested to prove the feasibility and robustness of the developed road marking extraction method. The average precision, recall, and F1-score obtained from four test datasets are 93.87%, 93.76%, and 93.73%, respectively. The accuracy assessment results demonstrate the practicability of the proposed method, which can successfully and accurately extract lane features from MLS point clouds. Furthermore, according to the buffer overlay analysis, the proposed algorithms were capable of achieving lane centerline generation with 30 cm wide localization accuracy with the assistance of 4 cm resolution UAV orthoimagery. Therefore, the proposed method can reliably and efficiently estimate lane centerlines in urban road environments from four MLS point cloud datasets in 30 cm localization accuracy. Our comparative analysis indicates that the proposed methods can achieve higher accuracy and robustness than most of state-of-the-art methods. Our future studies will focus on compound and spiral road curves such as roundabouts.

REFERENCES

[1] G. Bresson, Z. Alsayed, L. Yu, and S. Glaser, "Simultaneous localization and mapping: A survey of current trends in autonomous driving," *IEEE Trans. Intell. Vehicles*, vol. 2, no. 3, pp. 194–220, Sep. 2017.

[2] J.-F. Bonnefon, A. Shariff, and I. Rahwan, "The social dilemma of autonomous vehicles," *Science*, vol. 352, no. 6293, pp. 1573–1576, Jun. 2016.

[3] H. Chu, L. Guo, B. Gao, H. Chen, N. Bian, and J. Zhou, "Predictive cruise control using high-definition map and real vehicle implementation," *IEEE Trans. Veh. Technol.*, vol. 67, no. 12, pp. 11377–11389, Sep. 2018.

[4] H. Luo *et al.*, "Semantic labeling of mobile LiDAR point clouds via active learning and higher order MRF," *IEEE Trans. Geosci. Remote Sens.*, vol. 56, no. 7, pp. 3631–3644, Jul. 2018.

[5] W. Yao, S. Hinz, and U. Stilla, "Extraction and motion estimation of vehicles in single-pass airborne LiDAR data towards urban traffic analysis," *ISPRS J. Photogramm. Remote Sens.*, vol. 66, no. 3, pp. 260–271, May 2011.

[6] H. Fan, W. Yao, and L. Tang, "Identifying man-made objects along urban road corridors from mobile LiDAR data," *IEEE Geosci. Remote Sens. Lett.*, vol. 11, no. 5, pp. 950–954, May 2014.

[7] Y. Yu, J. Li, H. Guan, C. Wang, and C. Wen, "Bag of contextual-visual words for road scene object detection from mobile laser scanning data," *IEEE Trans. Intell. Transp. Syst.*, vol. 17, no. 12, pp. 3391–3406, Dec. 2016.

[8] Y. Yu, J. Li, H. Guan, and C. Wang, "Automated detection of three-dimensional cars in mobile laser scanning point clouds using DBM-hough-forests," *IEEE Trans. Geosci. Remote Sens.*, vol. 54, no. 7, pp. 4130–4142, Jul. 2016.

[9] L. Ma, Y. Li, J. Li, C. Wang, R. Wang, and M. Chapman, "Mobile laser scanned point-clouds for road object detection and extraction: A review," *Remote Sens.*, vol. 10, no. 10, p. 1531, Sep. 2018.

[10] Y. Xu *et al.*, "Classification of LiDAR point clouds using supervoxel-based detrended feature and perception-weighted graphical model," *IEEE J. Sel. Topics Appl. Earth Observ. Remote Sens.*, vol. 13, pp. 72–88, Feb. 2020.

[11] Y. Yu, J. Li, H. Guan, C. Wang, and J. Yu, "Semiautomated extraction of street light poles from mobile LiDAR point-clouds," *IEEE Trans. Geosci. Remote Sens.*, vol. 53, no. 3, pp. 1374–1386, Mar. 2015.

[12] E. Che, J. Jung, and M. Olsen, "Object recognition, segmentation, and classification of mobile laser scanning point clouds: A state of the art review," *Sensors*, vol. 19, no. 4, p. 810, Feb. 2019.

[13] B. Yang, Y. Liu, Z. Dong, F. Liang, B. Li, and X. Peng, "3D local feature BKD to extract road information from mobile laser scanning point clouds," *ISPRS J. Photogramm. Remote Sens.*, vol. 130, pp. 329–343, Aug. 2017.

This article has been accepted for inclusion in a future issue of this journal. Content is final as presented, with the exception of pagination.

YE *et al.*: ROBUST LANE EXTRACTION FROM MLS POINT CLOUDS TOWARDS HD MAPS ESPECIALLY IN CURVE ROAD

13

[14] P. Huang, M. Cheng, Y. Chen, H. Luo, C. Wang, and J. Li, "Traffic sign occlusion detection using mobile laser scanning point clouds," *IEEE Trans. Intell. Transport. Syst.*, vol. 18, no. 9, pp. 2364–2376, Sep. 2017.

[15] B. Yang, L. Fang, and J. Li, "Semi-automated extraction and delineation of 3D roads of street scene from mobile laser scanning point clouds," *ISPRS J. Photogramm. Remote Sens.*, vol. 79, pp. 80–93, May 2013.

[16] L. Yan, H. Liu, J. Tan, Z. Li, H. Xie, and C. Chen, "Scan line based road marking extraction from mobile LiDAR point clouds," *Sensors*, vol. 16, no. 6, p. 903, Jun. 2016.

[17] C. Cabo, A. Kukko, S. García-Cortés, H. Kaartinen, J. Hyyppä, and C. Ordoñez, "An algorithm for automatic road asphalt edge delineation from mobile laser scanner data using the line clouds concept," *Remote Sens.*, vol. 8, no. 9, p. 740, Sep. 2016.

[18] Y. Yu, J. Li, H. Guan, and C. Wang, "Automated extraction of urban road facilities using mobile laser scanning data," *IEEE Trans. Intell. Transport. Syst.*, vol. 16, no. 4, pp. 2167–2181, Aug. 2015.

[19] H. Guan, J. Li, Y. Yu, C. Wang, M. Chapman, and B. Yang, "Using mobile laser scanning data for automated extraction of road markings," *ISPRS J. Photogramm. Remote Sens.*, vol. 87, pp. 93–107, Jan. 2014.

[20] D. Zai *et al.*, "3-D road boundary extraction from mobile laser scanning data via supervoxels and graph cuts," *IEEE Trans. Intell. Transport. Syst.*, vol. 19, no. 3, pp. 802–813, Mar. 2018.

[21] B. Riveiro, H. González-Jorge, J. Martínez-Sánchez, L. Díaz-Vilariño, and P. Arias, "Automatic detection of zebra crossings from mobile LiDAR data," *Opt. Laser Technol.*, vol. 70, pp. 63–70, Jul. 2015.

[22] P. Kumar, P. Lewis, C. P. McElhinney, P. Boguslawski, and T. McCarthy, "Snake energy analysis and result validation for a mobile laser scanning data-based automated road edge extraction algorithm," *IEEE J. Sel. Topics Appl. Earth Observ. Remote Sens.*, vol. 10, no. 2, pp. 763–773, Feb. 2017.

[23] Y. Xu, R. Boerner, W. Yao, L. Hoegner, and U. Stilla, "Pairwise coarse registration of point clouds in urban scenes using voxel-based 4-planes congruent sets," *ISPRS J. Photogramm. Remote Sens.*, vol. 151, pp. 106–123, May 2019.

[24] S. Xu, R. Wang, and H. Zheng, "Road curb extraction from mobile LiDAR point clouds," *IEEE Trans. Geosci. Remote Sens.*, vol. 55, no. 2, pp. 996–1009, Feb. 2017.

[25] M. Cheng, H. Zhang, C. Wang, and J. Li, "Extraction and classification of road markings using mobile laser scanning point clouds," *IEEE J. Sel. Topics Appl. Earth Observ. Remote Sens.*, vol. 10, no. 3, pp. 1182–1196, Mar. 2017.

[26] M. Soilán, B. Riveiro, J. Martínez-Sánchez, and P. Arias, "Segmentation and classification of road markings using MLS data," *ISPRS J. Photogramm. Remote Sens.*, vol. 123, pp. 94–103, Jan. 2017.

[27] B. Yang, Z. Dong, Y. Liu, F. Liang, and Y. Wang, "Computing multiple aggregation levels and contextual features for road facilities recognition using mobile laser scanning data," *ISPRS J. Photogramm. Remote Sens.*, vol. 126, pp. 180–194, Apr. 2017.

[28] Y. Li, L. Li, D. Li, F. Yang, and Y. Liu, "A density-based clustering method for urban scene mobile laser scanning data segmentation," *Remote Sens.*, vol. 9, no. 4, p. 331, Mar. 2017.

[29] A. Kheyrollahi and T. P. Breckon, "Automatic real-time road marking recognition using a feature driven approach," *Mach. Vis. Appl.*, vol. 23, no. 1, pp. 123–133, Jan. 2012.

[30] N. Otsu, "A threshold selection method from gray-level histograms," *IEEE Trans. Syst., Man, Cybern.*, vol. SMC-9, no. 1, pp. 62–66, Jan. 1979.

[31] H. Guan, J. Li, Y. Yu, M. Chapman, and C. Wang, "Automated road information extraction from mobile laser scanning data," *IEEE Trans. Intell. Transport. Syst.*, vol. 16, no. 1, pp. 194–205, Feb. 2015.

[32] P. Kumar, C. P. McElhinney, P. Lewis, and T. McCarthy, "Automated road markings extraction from mobile laser scanning data," *Int. J. Appl. Earth Observ. Geoinf.*, vol. 32, pp. 125–137, Oct. 2014.

[33] I. Goodfellow, Y. Bengio, and A. Courville, *Deep Learning*. Cambridge, MA, USA: MIT Press, 2016.

[34] Z. Luo, J. Li, Z. Xiao, Z. G. Mou, X. Cai, and C. Wang, "Learning high-level features by fusing multi-view representation of MLS point clouds for 3D object recognition in road environments," *ISPRS J. Photogramm. Remote Sens.*, vol. 150, pp. 44–58, Apr. 2019.

[35] Y. Yu, J. Li, H. Guan, F. Jia, and C. Wang, "Learning hierarchical features for automated extraction of road markings from 3-D mobile LiDAR point clouds," *IEEE J. Sel. Topics Appl. Earth Observ. Remote Sens.*, vol. 8, no. 2, pp. 709–726, Feb. 2015.

[36] C. Wen, X. Sun, J. Li, C. Wang, Y. Guo, and A. Habib, "A deep learning framework for road marking extraction, classification and completion from mobile laser scanning point clouds," *ISPRS J. Photogramm. Remote Sens.*, vol. 147, pp. 178–192, Jan. 2019.

[37] Y. LeCun, Y. Bengio, and G. Hinton, "Deep learning," *Nature*, vol. 521, no. 7553, p. 436, 2015.

[38] A. Boyko and T. Funkhouser, "Extracting roads from dense point clouds in large scale urban environment," *ISPRS J. Photogramm. Remote Sens.*, vol. 66, no. 6, pp. S2–S12, Dec. 2011.

[39] A. Nurunnabi, G. West, and D. Belton, "Robust locally weighted regression techniques for ground surface points filtering in mobile laser scanning three dimensional point cloud data," *IEEE Trans. Geosci. Remote Sens.*, vol. 54, no. 4, pp. 2181–2193, Apr. 2016.

[40] B. Yang, Z. Dong, G. Zhao, and W. Dai, "Hierarchical extraction of urban objects from mobile laser scanning data," *ISPRS J. Photogramm. Remote Sens.*, vol. 99, pp. 45–57, Jan. 2015.

[41] J. Jung, E. Che, M. J. Olsen, and C. Parrish, "Efficient and robust lane marking extraction from mobile lidar point clouds," *ISPRS J. Photogramm. Remote Sens.*, vol. 147, pp. 1–18, Jan. 2019.

[42] X. Chen, B. Kohlmeyer, M. Stroila, N. Alwar, R. Wang, and J. Bach, "Next generation map making: Geo-referenced ground-level LIDAR point clouds for automatic retro-reflective road feature extraction," in *Proc. 17th ACM SIGSPATIAL Int. Conf. Adv. Geographic Inf. Syst. (GIS)*, 2009, pp. 488–491.

[43] J. Zhao, S. You, and J. Huang, "Rapid extraction and updating of road network from airborne LiDAR data," in *Proc. IEEE Appl. Imag. Pattern Recognit. Workshop (AIPR)*, Oct. 2011, pp. 1–7.

[44] X. Hu, Y. Li, J. Shan, J. Zhang, and Y. Zhang, "Road centerline extraction in complex urban scenes from LiDAR data based on multiple features," *IEEE Trans. Geosci. Remote Sens.*, vol. 52, no. 11, pp. 7448–7456, Nov. 2014.

[45] Z. Hui, Y. Hu, S. Jin, and Y. Z. Yevenyo, "Road centerline extraction from airborne LiDAR point cloud based on hierarchical fusion and optimization," *ISPRS J. Photogramm. Remote Sens.*, vol. 118, pp. 22–36, Aug. 2016.

Chengming Ye received the Ph.D. degree in Earth exploration and information technology from the Chengdu University of Technology, Chengdu, China, in 2011. He is currently an Associate Professor with the College of Geophysics, Chengdu University of Technology. He was a Visiting Scholar with the Department of Geography and Environmental Management, University of Waterloo, Canada, from 2016 to 2017. He has published more than 20 articles in peer-reviewed journals including the IEEE JOURNAL OF SELECTED TOPICS IN APPLIED EARTH OBSERVATIONS AND REMOTE SENSING (JSTARS). His main research interests include geo-hazard remote sensing applications, ecological remote sensing, and LiDAR data processing.

He Zhao received the B.Eng. degree in electrical engineering from Qingdao University, China, in 2015, and the M.Sc. degree in geomatics from the University of Waterloo, Canada, in 2017. His M.Sc. thesis was about the development of the algorithms and software tools for creating HD maps using mobile laser scanning (MLS) point clouds to support autonomous vehicles. He has been with SenseTime Inc., Shanghai, China, since 2017. His research interests include artificial intelligence, machine learning, HD maps, and urban remote sensing.

Lingfei Ma (Graduate Student Member, IEEE) received the B.Sc. degree in GiScience from the China University of Geoscience, Beijing, China, in 2015, and the B.Sc. and M.Sc. degrees in geomatics from the University of Waterloo, Canada, in 2015 and 2017, respectively. He is currently pursuing the Ph.D. degree in remote sensing with the Mobile Sensing and Geodata Science Laboratory. His research interests include autonomous driving, HD mapping, mobile LiDAR, point cloud processing, 3D scene modeling, and deep learning.

Han Jiang received the B.Sc. degree in GiScience from the China University of Geosciences, Beijing, China, in 2015, and the M.Sc. degree in geomatics from the University of Waterloo, Canada, in 2017. His M.Sc. thesis was entitled Semi-automated generation of road transition lines using mobile laser scanning data. His research interests include mobile LiDAR, point cloud processing, HD maps for autonomous vehicles, deep learning, and AI.

Hongfu Li received the B.Eng. degree in space science and technology from the Chengdu University of Technology, China, in 2019, where he is currently pursuing the master's degree in Earth exploration and information technology. His main research interests comprise geo-hazard remote sensing applications, mobile LiDAR, point cloud processing, and deep learning.

Ruisheng Wang (Senior Member, IEEE) received the B.Eng. degree in photogrammetry and remote sensing from Wuhan University, China, the M.Sc.E. degree in geomatics engineering from the University of New Brunswick, Canada, and the Ph.D. degree in electrical and computer engineering from McGill University, Canada.

He is currently an Associate Professor with the Department of Geomatics Engineering, University of Calgary. Prior to that, he worked as an Industrial Researcher at HERE (formerly NAVTEQ) in Chicago, USA, from 2008 to 2012. His researches interests include mobile LiDAR data processing for next generation map making, AI algorithms for point cloud processing, and navigation. He has published more than 60 research articles in peer-reviewed journals including *ISPRS Journal of Photogrammetry and Remote Sensing*, the IEEE TRANSACTIONS ON GEO-SCIENCES AND REMOTE SENSING, and the IEEE JOURNAL OF SELECTED TOPICS IN APPLIED EARTH OBSERVATIONS AND REMOTE SENSING (JSTARS). He is an Associate Editor of the *Journal of Applied Remote Sensing* and *Photogrammetric Engineering and Remote Sensing*.

Michael A. Chapman received the Ph.D. degree in photogrammetry from Laval University, Quebec City, QC, Canada.

He is currently a Professor of geomatics engineering with the Department of Civil Engineering, Ryerson University, Toronto, ON, Canada. Prior to joining Ryerson University, he was a Professor with the Department of Geomatics Engineering, University of Calgary, Canada, for 18 years. He has authored or coauthored over 200 technical articles. His research interests include algorithms and processing methodologies for airborne sensors using global navigation satellite system (GNSS) and inertial measurement unit (IMU), geometric processing of digital imagery in industrial environments, terrestrial imaging systems for transportation infrastructure mapping, mobile mapping for HD maps, and algorithms and processing strategies for bio-metrology applications.

José Marcato Junior (Member, IEEE) received the Ph.D. degree in cartographic science from Sao Paulo State University, Brazil.

He is currently a Professor with the Faculty of Engineering, Architecture and Urbanism and Geography, Federal University of Mato Grosso do Sul, Campo Grande, Brazil. His current research interests include UAV photogrammetry and deep neural networks for object detection, classification and segmentation. He has published more than 30 articles in refereed journals and over 70 papers in conferences, including articles published in *ISPRS Journal of Photogrammetry and Remote Sensing*, the IEEE JOURNAL OF SELECTED TOPICS IN APPLIED EARTH OBSERVATIONS, *Remote Sensing*, *Sensors*, and *The Photogrammetric Record*.

Jonathan Li (Senior Member, IEEE) received the Ph.D. degree in geomatics engineering from the University of Cape Town, Cape Town, South Africa. He is currently a Professor and the Head of the Mobile Sensing and Geodata Science Group, Department of Geography and Environmental Management, University of Waterloo, Canada. He has coauthored more than 400 publications, more than 200 of which were published in refereed journals, including the IEEE TRANSACTIONS ON GEOSCIENCE AND REMOTE SENSING (TGRS), the IEEE TRANSACTIONS ON INTELLIGENT TRANSPORTATION SYSTEMS (TITS), the IEEE JOURNAL OF SELECTED TOPICS IN APPLIED EARTH OBSERVATIONS AND REMOTE SENSING (JSTARS), ISPRS-JPRS, and RSE. His research interests include information extraction from LiDAR point clouds and from earth observation images. He is the Chair of the ISPRS WG I/2 on LiDAR, Air- and Space-borne Optical Sensing from 2016 to 2020 and the ICA Commission on Sensor-Driven Mapping for the period of 2019–2023, and the Associate Editor of the IEEE TRANSACTIONS ON INTELLIGENT TRANSPORTATION SYSTEMS, the IEEE JOURNAL OF SELECTED TOPICS IN APPLIED EARTH OBSERVATIONS AND REMOTE SENSING, and *Canadian Journal of Remote Sensing*.